ACS APPLIED MATERIALS & INTERFACES

Research Article

Cite This: ACS Appl. Mater. Interfaces 2018, 10, 10771−10777

www.acsami.org

Pt/TiSi$_x$-NCNT Novel Janus Nanostructure: A New Type of High-Performance Electrocatalyst

Gaixia Zhang,[†,‡] Mohammad Norouzi Banis,[†] Qiliang Wei,[‡] Mei Cai,[§] Yong Zhang,[†] Ruying Li,[†] Shuhui Sun,[*,†,‡] and Xueliang Sun[*,†]

[†]Department of Mechanical and Materials Engineering, University of Western Ontario, London, Ontario N6A 5B9, Canada

[‡]Institut National de la Recherche Scientifique-Énergie Matériaux et Télécommunications, Varennes, QC J3X 1S2, Canada

[§]General Motors Research and Development Center, Warren, Michigan 48090-9055, United States

Supporting Information

ABSTRACT: Novel Janus nanostructured electrocatalyst (Pt/TiSi$_x$-NCNT) was prepared by first sputtering TiSi$_x$ on one side of N-doped carbon nanotubes (NCNTs), followed by wet chemical deposition of Pt nanoparticles (NPs) on the other side. Transmission electron microscopy (TEM) studies showed that the Pt NPs are mainly deposited on the NCNT surface where no TiSi$_x$ (i.e., between the gaps of TiSi$_x$ film). This feature could benefit the increase in the stability of the Pt NP catalyst. Indeed, compared to the state-of-the-art commercial Pt/C catalyst, this novel Pt/TiSi$_x$-NCNT Janus structure showed ∼3 times increase in stability as well as significantly improved CO tolerance. The obvious performance enhancement could be attributed to the better corrosion resistance of TiSi$_x$ and NCNTs than the carbon black that is used in the commercial Pt/C catalyst. Pt/TiSi$_x$-NCNT Janus nanostructures open the door for designing new type of high-performance electrocatalyst for fuel cells and other oxygen reduction reaction-related energy devices.

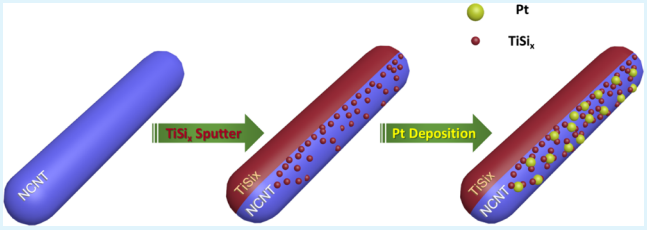

KEYWORDS: *Janus nanostructures, electrocatalyst, stability, CO tolerance, fuel cells*

INTRODUCTION

Because of their high efficiency, high power density, and zero emission, polymer electrolyte membrane (PEM) fuel cells (PEMFCs) are a type of promising power sources being developed for transportation, stationary and portable device applications.[1] Despite much progress achieved, the high cost and insufficient stability of Pt-based catalysts are two of the key challenges that are hindering the wide-spread commercialization of PEMFCs.[2−4] Pt and Pt-based catalysts are commonly used in both anode (for oxidation of hydrogen, methanol, ethanol, etc.) and cathode [for oxygen reduction reaction (ORR)] in PEMFCs.[5,6] In the literature, different carbon materials, such as carbon black spheres,[7,8] carbon nanofibers,[9] and carbon nanotubes,[10,11] have been widely reported as catalyst supports because of their high surface area and good electrical conductivity. It is well-accepted that the performance degradation of PEMFCs could be attributed to the following factors: (1) the dissolution, aggregation, Oswald ripening, and poisoning of Pt catalysts and (2) the corrosion (electrochemical oxidation) of the carbon supports during fuel cell operation, especially at potentials higher than 0.9 V.[12−14] To address these challenges, researchers have employed various materials, including carbide, nitride, and metal oxide, as alternative catalyst supports because of their better stability and/or stronger interaction with Pt than carbon black support.[15,16]

Because of their excellent corrosion resistance, thermal stability, and electrical conductivity,[17−19] metal silicides (e.g., TiSi$_x$) have recently attracted much interest as alternative catalyst supports in PEMFCs. Metal silicide-supported Pt catalysts have been reported to show improved stability and activity for ORR and methanol oxidation.[20,21] Most of the previously reported metal silicides were in the form of thin films or powders, which hardly provide high surface area demanded for using as catalyst supports. The combination of TiSi$_x$ and carbon materials as supports potentially allows the optimization of the dispersion and corrosion.

Herein, we have developed a new type of electrocatalyst by combining N-doped carbon nanotubes (NCNTs) and TiSi$_x$ as the Pt support. As demonstrated in Figure 1, this strategy was realized by a two-step method, specifically, TiSi$_x$ was first sputtered onto one side of NCNTs, and then Pt nanoparticles (NPs) were deposited on the other side through wet chemical reduction, forming a unique one-dimensional Janus nanostructure (Pt/TiSi$_x$-NCNT). Ever since Gennes first emphasized the Janus structure in his Nobel Prize address,[22] this unique nanostructure has attracted increasing interests in various applications.[23] In general, Janus structures include two different

Received: October 15, 2017
Accepted: March 6, 2018
Published: March 6, 2018

DOI: 10.1021/acsami.7b15682
ACS Appl. Mater. Interfaces 2018, 10, 10771−10777

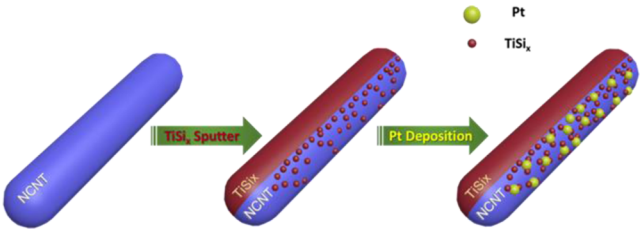

Figure 1. Schematic illustration of the fabrication process of PtNP/$TiSi_x$-NCNT Janus nanostructures.

materials on the opposite faces and thus possess dual surface properties.[24] Therefore, this type of unique Janus nanostructure has promising applications in drug delivery, biosensing, catalysis, and so forth. Moreover, in this work, Pt/$TiSi_x$-NCNT Janus nanostructures were directly grown on a carbon paper, which is commonly used as fuel cell backing, forming novel three-dimensional (3D) nanostructured electrodes. Importantly, such 3D supports possess additional advantages, such as improved mass transport, better gas permeability, and increased catalyst−support interaction.

EXPERIMENTAL SECTION

Preparation of $TiSi_x$-NCNT Catalyst Support. Chemical vapour deposition (CVD) and magnetron sputtering techniques have been combined to fabricate the $TiSi_x$-NCNT nanostructure. In this work, NCNTs were first grown on a carbon paper via a CVD process at 800 °C. The carbon paper was precoated with an Al buffer layer (30 nm) and a Fe catalyst layer (1 nm). For the NCNT synthesis, melamine was used as the precursor for both carbon and nitrogen sources.[25] After that, the carbon paper with NCNTs was put in a plasma-enhanced CVD/sputtering system. To purge the oxygen in the system, the pressure in the chamber was vacuumed down to 1.9×10^{-5} Torr, and then Ar gas was introduced into the chamber to tune the pressure to 1.5×10^{-3} Torr. The Ar flow rate was kept at 15 sccm during sputtering. A $TiSi_x$ thin layer (100 nm) was deposited on the NCNTs by using a $TiSi_2$ target (2 in.) under radio frequency magnetron (150 W, 10 min).

Preparation of Pt/$TiSi_x$-NCNT Janus Nanostructure. Pt NPs were deposited on $TiSi_x$/NCNTs through the reduction of hexachloroplatinic acid ($H_2PtCl_6{\cdot}6H_2O$) at 80 °C by formic acid (HCOOH).[26] In a typical experiment, $H_2PtCl_6{\cdot}6H_2O$ (32 mg, Aldrich), HCOOH (Aldrich, 1 mL), and H_2O (20 mL) were mixed in a glass vial at room temperature. The $TiSi_x$/NCNT/carbon paper substrate was immersed into the above reaction solution, and then the vial was place in a water bath (80 °C) for 30 min. After reaction, the carbon paper sample was washed with deionized water three times and dried in a vacuum oven. Inductively coupled plasma (ICP)−optical emission spectroscopy was used to evaluate the Pt loadings in the samples.

Physical Characterization. The as-synthesized samples were characterized by scanning electron microscopy (SEM, Hitachi S-4800, operated at 5 kV), transmission electron microscopy (TEM, JEOL JEM-2100, operated at 200 kV), and X-ray diffraction (Bruker D8 ADVANCE diffractometer equipped with a Cu Kα radiation source).

Electrochemical Evaluations. Cyclic voltammetry (CV) measurements of the Pt/$TiSi_x$-NCNT/carbon paper were conducted in a standard three-electrode cell at room temperature, using Ag/AgCl (3 M NaCl) and Pt wire as the reference and counter electrodes, respectively. All potentials in this work, however, are normalized to the reversible hydrogen electrode (RHE). CV measurements were conducted in a N_2-saturated 0.5 M H_2SO_4 solution at a scan rate of 50 mV/s by using a CHI 600C (CH Instrument Company) system. The 4000 cycle accelerated durability test (ADT) was performed by potential cycling between 0.60 and 1.2 V at 50 mV/s in a O_2-saturated 0.5 M H_2SO_4 solution at room temperature. Meanwhile, the full-scale CV between 0.0 and 1.2 V in N_2-saturated H_2SO_4 solution (0.5 M) was taken periodically to track the degradation of the three Pt-based catalysts. The electrochemical active surface areas (ECSAs) of the Pt catalysts were calculated from the hydrogen adsorption peaks in the CV curves. For methanol oxidation properties, the CV measurements were conducted in an N_2-saturated 0.5 M H_2SO_4 solution containing 1 M MeOH. For CO-stripping measurements, pure CO (99.5%) was purged into the solution for 1 h, with the electrode polarized at 0.05 V (vs. RHE) in a fume hood. Then the solution was purged with ultrahigh pure N_2 for another 1 h under potential control, followed by voltammetric stripping.

For comparison purpose, other materials including $TiSi_x$-NCNT, PtNP/NCNT, and 30 wt % Pt/C (ETEK) were also evaluated under identical conditions. To prepare the ETEK Pt/C electrode, 10 mg of the catalyst was put in 1 mL of H_2O/isopropanol (1/1 in volume ratio) solution and then sonicated for 30 min to make a uniform ink suspension. The glassy carbon (GC) disk electrodes (5 mm in diameter) were polished to a mirror finish before using. The catalyst suspension (20 μL) was dropped onto the GC disk electrode and then dried under N_2 flow. Then, 10 μL of Nafion solution (0.05 wt %) was dropped onto the catalyst film. For the Pt/C catalyst, the Pt loading on the GC electrode was maintained at 0.3058 mg/cm^2, which is similar to the Pt loading for the PtNP/$TiSi_x$-NCNT electrode (measured through ICP).

RESULTS AND DISCUSSION

The surface morphology change of the NCNTs before and after $TiSi_x$ sputtering can be clearly seen from the SEM and TEM images in Figure 2. The pristine NCNTs have diameters

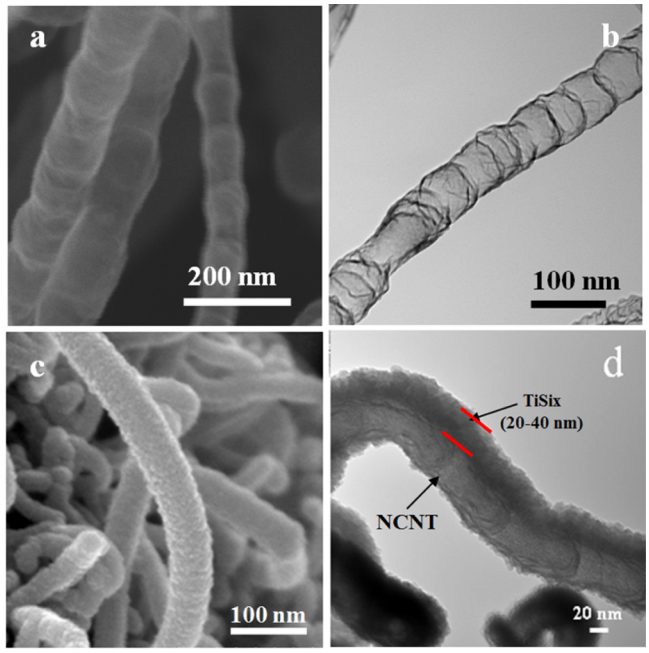

Figure 2. SEM (a,c) and TEM (b,d) images of NCNTs with (a,b) and without (c,d) $TiSi_x$ coating.

of 40 to 60 nm (Figure 2a,b), and the CNT surfaces are relatively smooth and possess a bamboolike structure, which is due to N-doping, that is, the integration of N into the graphitic structure. After the $TiSi_x$ film deposition via sputtering, the NCNTs surface became very rough, and the bamboolike structure is also difficult to be seen. Impressively, after the $TiSi_x$ coating, the NCNTs still kept their "free-standing" 3D architecture (Figure 2c). The TEM image (Figure 2d) indicates that the $TiSi_x$ film (20−40 nm) only covers one side of the NCNTs, leaving the other parts either without the $TiSi_x$ film or

DOI: 10.1021/acsami.7b15682
ACS Appl. Mater. Interfaces 2018, 10, 10771−10777

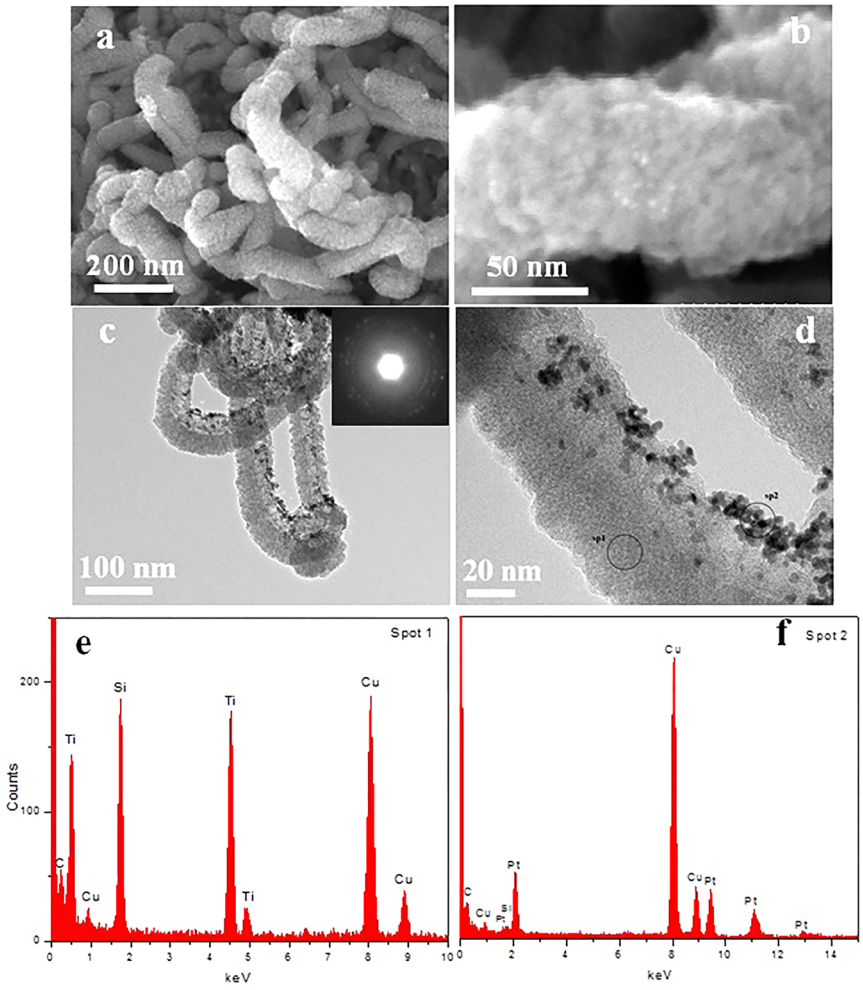

Figure 3. SEM (a,b) and TEM (c,d) images of Pt NPs deposited on $TiSi_x$-NCNTs. (e,f) EDX spectra recorded from different selected areas, sp^1 and sp^2, respectively, in (d).

partially covered with a very thin particle film. This phenomenon might be caused by the shadow effect of the sputtering process.

Interestingly, after Pt deposition (Figure 3a–d), the Pt NPs deposit, selectively, on the surface of NCNTs, which has no $TiSi_x$ coating, forming a unique PtNP/$TiSi_x$-NCNT Janus nanostructure. This might be caused by the inert surface of the $TiSi_x$ film, which is hard for Pt attachment. On the contrary, for pristine NCNT support, the Pt NPs (3–4 nm in diameter) distribute relatively uniformly on their whole surface (Figure S1). The inset in Figure 3c shows the selected area electron diffraction patterns, which reveal the crystallinity and amorphous nature of the Pt NPs and the $TiSi_x$ film, respectively. Figure 3e,f shows the energy-dispersive X-ray (EDX) spectra taken from two selected areas, indicated by cycles 1 and 2 in Figure 3d, of the Pt/$TiSi_x$-NCNT Janus nanostructure. The EDX results further confirm that $TiSi_x$ deposits on one side while Pt deposits on the opposite side of NCNTs. Figure 4a,b show the high-resolution TEM (HRTEM) images of the sample at different magnifications and locations, which further demonstrate the highly crystalline character of Pt NPs and also the amorphous phase of the $TiSi_x$ film. The 0.23 nm lattice spacing of Pt corresponds to the Pt(111) plane of the face-centered-cubic structure. The 0.34 nm lattice spacing can be indexed to the (002) plane of the CNTs. Moreover, in some places, Pt NPs preferentially grow between the gaps of

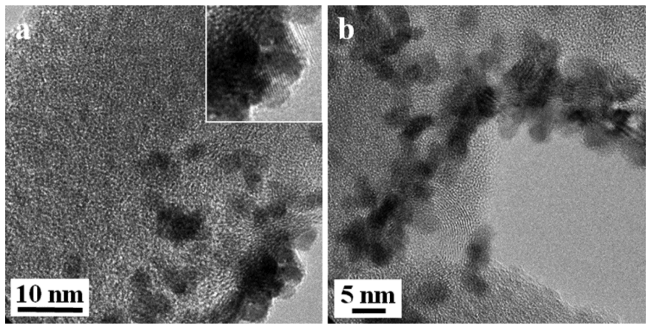

Figure 4. HRTEM images (a,b) of PtNP/$TiSi_x$-NCNTs at different magnifications and locations.

$TiSi_x$ film/nanoparticles, and then form elongated dendritic or chainlike Pt nanostructures.

The electrochemical properties of the Pt/$TiSi_x$-NCNT Janus nanostructures were evaluated via CV. For comparison purpose, the pristine $TiSi_x$-NCNT (no Pt) and commercial Pt/C (ETEK) were also evaluated under identical conditions. The CVs were recorded between 0 and 1.2 V versus RHE in N_2-saturated 0.5 M H_2SO_4 solution with a scan rate of 50 mV/s. From Figure 5, we can see that $TiSi_x$-NCNT only shows the background currents representing the characteristic of CNT electrodes (black line), indicating that the $TiSi_x$-NCNT support

DOI: 10.1021/acsami.7b15682
ACS Appl. Mater. Interfaces 2018, 10, 10771–10777

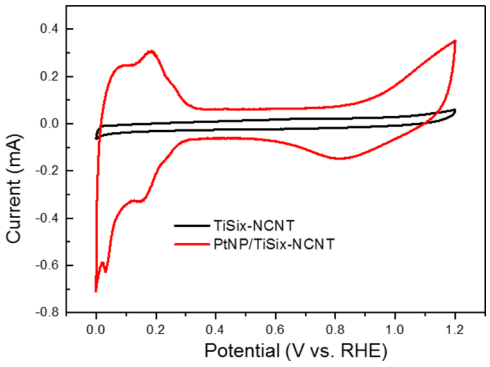

Figure 5. CVs of pristine $TiSi_x$-NCNT (black curve) and PtNP/$TiSi_x$-NCNT (red curve). Measured in N_2-saturated 0.5 M H_2SO_4 with a scan rate of 50 mV/s.

itself is not active. The Pt/$TiSi_x$-NCNT electrode shows clear and characteristic Pt surface electrochemistry (red line), that is, the hydrogen adsorption and desorption peaks between 0 and 0.3 V and Pt oxidation and reduction peaks between 0.75 and 1.2 V. Moreover, it also shows the multiple peaks for hydrogen adsorption and desorption, indicating that multiple exposed Pt crystallographic planes were involved in the reaction.[8]

ADT was conducted to evaluate the durability of the catalysts. Linear potential sweeps were continuously applied to initiate the surface oxidation/reduction of Pt and also the oxidation of the Pt support. The formation of PtOH and PtO on the Pt surface induces the dissolution of Pt through the Pt^{2+} oxidation state.[27] The ADT tests were performed by applying linear potential sweeps from 0.6 to 1.2 V (vs RHE) with a scan rate of 50 mV/s in O_2-saturated 0.5 M H_2SO_4 solution at room temperature. After 4000 cycles, the ECSAs of the Pt-based catalyst were determined by measuring the H adsorption and compared with the ECSAs before ADT cycling. From Figure 6a,d, we can see that the commercial Pt/C (ETEK) catalyst lost 67.5% of its initial ECSA, whereas impressively, the Janus nanostructured Pt/$TiSi_x$-NCNT catalyst only lost 20% of its original Pt ECSA (Figure 6c,d); in other words, Pt/$TiSi_x$-NCNT is 3.4 times more stable than the commercial Pt/C catalyst. To further investigate the role of $TiSi_x$ coating, Pt NPs were grown on pristine NCNTs without $TiSi_x$ coating, and the ADT tests were conducted under identical conditions. As shown in Figure 6b,d, after 4000 cycles ADT test, PtNP/NCNTs lost 56.5% of the original Pt surface area. We can see that on the same NCNT support, with the addition of $TiSi_x$, the stability of Pt was significantly increased by 2.8-fold.

Clearly, the Janus nanostructured Pt/$TiSi_x$-NCNT exhibits the best stability among the three samples, followed by the Pt/NCNT sample that shows better stability than the commercial Pt/C catalyst. The significant stability increase could be attributed to the following factors: first, NCNTs possess a higher corrosion resistance than the carbon black used in the Pt/C commercial catalyst,[28] and moreover, by adding the more corrosion resistant $TiSi_x$, the stability of the Pt/$TiSi_x$-NCNT catalyst was further increased. Second, Pt NPs sit between the gaps of $TiSi_x$, which act as an energy barrier to alleviate the migration/aggregation of individual Pt NPs (as shown in Figure 1).[29] Third, the unique dendritic and chainlike structure of Pt makes it less vulnerable to Ostwald ripening and aggregation during cycling than the PtNPs.[8] Therefore, the Pt/$TiSi_x$-NCNT Janus catalyst is much more stable than the commercial Pt/C catalyst.

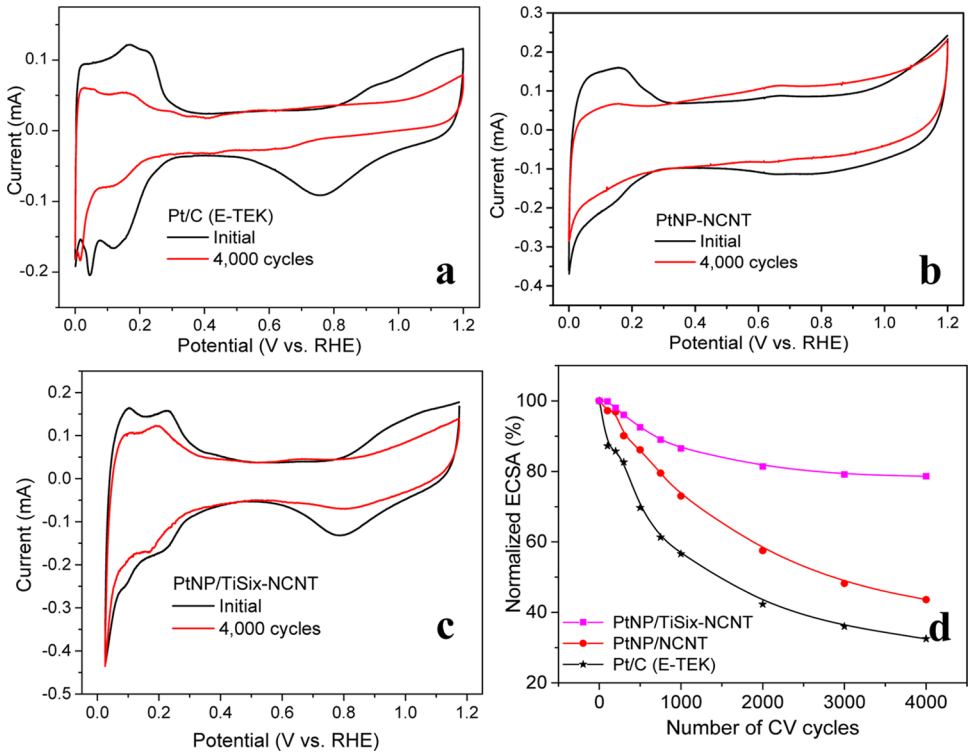

Figure 6. CV curves for catalysts before (black curve) and after (red curve) 4000 cycles ADT test: (a) Pt/C (E-TEK), (b) PtNP/NCNT, and (c) PtNP/$TiSi_x$-NCNT catalysts. (d) ECSA loss of the three catalysts as a function of the cycling numbers in O_2-saturated H_2SO_4 solution (0.5 M) at room temperature.

DOI: 10.1021/acsami.7b15682
ACS Appl. Mater. Interfaces 2018, 10, 10771−10777

The electrocatalytic activity for methanol oxidation reaction (MOR) of the Pt/TiSi$_x$-NCNT was evaluated in 0.5 M H_2SO_4 solution containing 1 M MeOH. For comparison, the MOR properties of the pristine TiSi$_x$-NCNT and commercial Pt/C were also studied under identical conditions. As shown in the voltammograms (curve a) in Figure 7, no obvious methanol

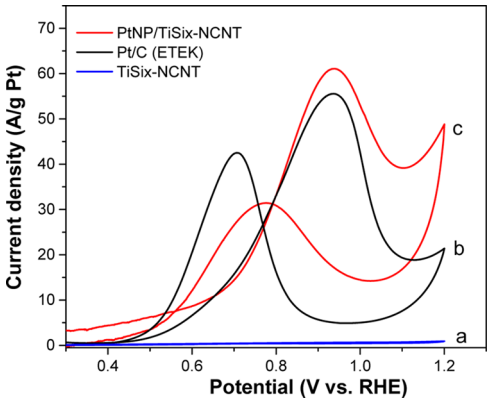

Figure 7. CVs for MOR (1 M methanol in 0.5 M H_2SO_4). Trace (a,b,c) represents TiSi$_x$-NCNT, Pt/C, and PtNP/TiSi$_x$-NCNT, respectively.

oxidation peaks could be seen from the CV of the TiSi$_x$-NCNT electrode, which means that the TiSi$_x$-NCNT support itself is not active for methanol oxidation. For Pt/C (curve b) and Pt/TiSi$_x$-NCNT (curve c), there are two typical oxidation peaks appearing from the CV curves, which are due to the oxidations of methanol and their intermediates.[30] After normalization to Pt loading, in the forward scan, Pt/TiSi$_x$-NCNT shows higher activity (62.0 A/g$_{Pt}$) for methanol oxidation than that (56 A/g$_{Pt}$) the ETEK Pt/C catalyst. According to Goodenough et al.,[31] the anodic peak in the reverse scan could be due to the removal of the incomplete oxidized carbonaceous species, for example, HCOO−, CO, or HCO−, which were accumulated on the Pt surface during the forward scan. Therefore, the current density ratio between the forward scan and the backward scan, I_f/I_b, are commonly used to evaluate the catalyst CO tolerance capability. A higher I_f/I_b ratio indicates the improved CO tolerance, whereas a lower I_f/I_b value usually means poor activity for the oxidation of methanol and the excessive accumulation of residual carbon species on the Pt surface. In our work, Pt/TiSi$_x$-NCNT Janus nanostructure shows a much higher I_f/I_b value than that of Pt/C catalyst (2.0 vs 1.3), suggesting that methanol could be oxidized more effectively on the Pt/TiSi$_x$-NCNT catalyst during the forward scan, while releasing less poisoning species than the commercial Pt/C catalyst, that is, Pt/TiSi$_x$-NCNT has better CO tolerance than commercial Pt/C catalyst.

To further investigate the CO tolerance properties of the samples, CO-stripping voltammograms were conducted on the three samples: Pt/C, Pt/NCNT, and Pt/TiSi$_x$-NCNT catalysts. CO adsorption was performed via holding the potential at 0.05 V (vs. RHE) for 20 min. Figure 8 shows that, for the three catalysts, there was a sharp peak during the first scan (red line), whereas it disappeared in the subsequent scan (black line). This indicates that the monolayer CO adsorbed on the Pt surface was completely oxidized during the first forward scan. The peak potential for CO oxidation on Pt/C, Pt/NCNT, and Pt/TiSi$_x$-NCNT catalysts are located at 0.867, 0.862, and 0.837 V (vs RHE), respectively. The results indicate that the Pt/TiSi$_x$-NCNT Janus nanostructure is more tolerant to CO poisoning,

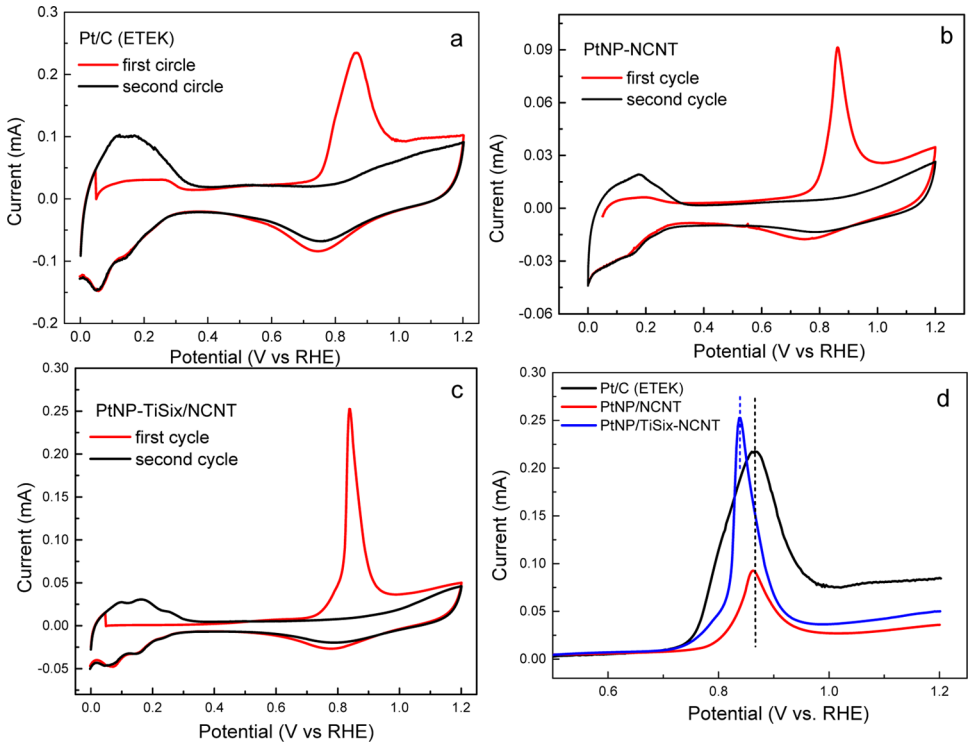

Figure 8. CO stripping of (a) Pt/C, (b) PtNP/NCNT, (c) PtNP/TiSi$_x$-NCNT in the presence of CO in 0.5 M H_2SO_4 solution. Scan rate: 50 mV/s. For the three catalysts, a sharp peak appears in the first scan (red line) and disappears during the subsequent scan (black line). (d) For the commercial Pt/C catalyst, the CO-stripping peak potential centers at 0.867 V, whereas it centers at 0.837 V for PtNP/TiSi$_x$-NCNT.

DOI: 10.1021/acsami.7b15682
ACS Appl. Mater. Interfaces 2018, 10, 10771−10777

which may due to the involvement of $TiSi_x$. Previous studies have demonstrated that using metal oxide nanostructures as Pt catalyst supports could increase the CO tolerance of the Pt. This is because, according to a so-called bifunctional mechanism, metal oxide could provide oxygen containing (e.g., −OH) groups which help in removing the strongly absorbed species such as CO.[31−35] Thus, the much improved CO tolerance of the Pt/$TiSi_x$-NCNT Janus nanostructure may originate from the $TiSi_x$ coating, which could provide oxygen-containing (e.g. −OH) groups on the catalyst surface.

CONCLUSIONS

In summary, a simple two-step method has been developed to fabricate a novel Pt/$TiSi_x$-NCNT Janus nanostructure, which consists of NCNTs with deposition of $TiSi_x$ on one side and Pt NPs on the other side. The Pt/$TiSi_x$-NCNT Janus nanocatalyst showed a much enhanced (~3 times) stability and CO tolerance compared to the commercial Pt/C catalyst. Pt/$TiSi_x$-NCNT Janus nanostructures provide a new strategy to design next-generation high-performance electrocatalyst for fuel cells and other energy devices.

ASSOCIATED CONTENT

Supporting Information

The Supporting Information is available free of charge on the ACS Publications website at DOI: 10.1021/acsami.7b15682.

SEM and TEM images of Pt NPs on NCNTs (PDF)

AUTHOR INFORMATION

Corresponding Authors

*E-mail: shuhui@emt.inrs.ca (S.S.).
*E-mail: xsun9@uwo.ca (X.S.).

ORCID

Mohammad Norouzi Banis: 0000-0002-6144-6837
Shuhui Sun: 0000-0002-0508-2944

Author Contributions

The manuscript was written through contributions of all authors. All authors have given approval to the final version of the manuscript.

Notes

The authors declare no competing financial interest.

ACKNOWLEDGMENTS

This work was supported by General Motors (GM) of Canada, Natural Sciences and Engineering Research Council of Canada (NSERC), the University of Western Ontario, the Institut National de la Recherche Scientifique (INRS), and the Fonds de recherche du Québec−Nature et technologies (FRQNT).

REFERENCES

(1) He, D.; Tang, H.; Kou, Z.; Pan, M.; Sun, X.; Zhang, J.; Mu, S. Engineered Graphene Materials: Synthesis and Applications for Polymer Electrolyte Membrane Fuel Cells. *Adv. Mater.* **2017**, *29*, 1601741.

(2) Wang, Y.-J.; Fang, B.; Li, H.; Bi, X. T.; Wang, H. Progress in Modified Carbon Support Materials for Pt and Pt-Alloy Cathode Catalysts in Polymer Electrolyte Membrane Fuel Cells. *Prog. Mater. Sci.* **2016**, *82*, 445−498.

(3) Arumugam, B.; Tamaki, T.; Yamaguchi, T. Beneficial Role of Copper in the Enhancement of Durability of Ordered Intermetallic PtFeCu Catalyst for Electrocatalytic Oxygen Reduction. *ACS Appl. Mater. Interfaces* **2015**, *7*, 16311−16321.

(4) Gasteiger, H. A.; Kocha, S. S.; Sompalli, B.; Wagner, F. T. Activity Benchmarks and Requirements for Pt, Pt-Alloy, and Non-Pt Oxygen Reduction Catalysts for PEMFCs. *Appl. Catal., B* **2005**, *56*, 9−35.

(5) Brandon, N. P.; Skinner, S.; Steele, B. C. H. Recent Advances in Materials for Fuel Cells. *Annu. Rev. Mater. Res.* **2003**, *33*, 183−213.

(6) Xu, W.; Wu, Z.; Tao, S. Recent Progress in Electrocatalysts with Mesoporous Structures for Application in Polymer Electrolyte Membrane Fuel Cells. *J. Mater. Chem. A* **2016**, *4*, 16272−16287.

(7) Zhou, Z.; Wang, S.; Zhou, W.; Wang, G.; Jiang, L.; Li, W.; Song, S.; Liu, J.; Sun, G.; Xin, Q. Novel Synthesis of Highly Active Pt/C Cathode Electrocatalyst for Direct Methanol Fuel Cell. *Chem. Commun.* **2003**, 394−395.

(8) Sun, S.; Zhang, G.; Geng, D.; Chen, Y.; Li, R.; Cai, M.; Sun, X. A New Highly Durable Pt Nanocatalyst for PEM Fuel Cells: the Multiarmed Star-Like Nanowire Single Crystal. *Angew. Chem., Int. Ed.* **2011**, *50*, 422−426.

(9) Zheng, J.-S.; Wang, M.-X.; Zhang, X.-S.; Wu, Y.-X.; Li, P.; Zhou, X.-G.; Yuan, W.-K. Platinum/Carbon Nanofiber Nanocomposite Synthesized by Electrophoretic Deposition As Electrocatalyst for Oxygen Reduction. *J. Power Sources* **2008**, *175*, 211−216.

(10) Guo, S.; Dong, S.; Wang, E. Au/Pt Hybrid Nanoparticles Supported on Multiwalled Carbon Nanotube/Silica Coaxial Nanocables: Preparation and Application As Electrocatalysts for Oxygen Reduction. *J. Phys. Chem. C* **2008**, *112*, 2389−2393.

(11) Sun, S.; Yang, D.; Zhang, G.; Sacher, E.; Dodelet, J.-P. Synthesis and Characterization of Carbon Nanotube−Pt Nanowire Heterostructures. *Chem. Mater.* **2007**, *19*, 6376−6378.

(12) Borup, R.; Meyers, J.; Pivovar, B.; Kim, Y. S.; Mukundan, R.; Garland, N.; Myers, D.; Wilson, M.; Garzon, F.; Wood, D.; Zelenay, P.; More, K.; Stroh, K.; Zawodzinski, T.; Boncella, J.; McGrath, J. E.; Inaba, M.; Miyatake, K.; Hori, M.; Ota, K.; Ogumi, Z.; Miyata, S.; Nishikata, A.; Siroma, Z.; Uchimoto, Y.; Yasuda, K.; Kimijima, K.-i.; Iwashita, N. Scientific Aspects of Polymer Electrolyte Fuel Cell Durability and Degradation. *Chem. Rev.* **2007**, *107*, 3904−3951.

(13) Shao, Y.; Yin, G.; Gao, Y. Understanding and Approaches for The Durability Issues of Pt-Based Catalysts for PEM Fuel Cell. *J. Power Sources* **2007**, *171*, 558−566.

(14) Saha, M. S.; Li, R.; Sun, X. High Loading and Monodispersed Pt Nanoparticles on Multiwalled Carbon Nanotubes for High Performance Proton Exchange Membrane Fuel Cells. *J. Power Sources* **2008**, *177*, 314−322.

(15) Shao, Y.; Liu, J.; Wang, Y.; Lin, Y. Novel Catalyst Support Materials for PEM Fuel Cells: Current Status and Future Prospects. *J. Mater. Chem.* **2009**, *19*, 46−59.

(16) Gasteiger, H. A.; Kocha, S. S.; Sompalli, B.; Wagner, F. T. Activity Benchmarks and Requirements for Pt, Pt-Alloy, and Non-Pt Oxygen Reduction Catalysts for PEMFCs. *Appl. Catal., B* **2005**, *56*, 9−35.

(17) Schmitt, A. L.; Higgins, J. M.; Szczech, J. R.; Jin, S. Synthesis and Applications of Metal Silicide Nanowires. *J. Mater. Chem.* **2010**, *20*, 223−235.

(18) Zhou, S.; Liu, X.; Lin, Y.; Wang, D. Spontaneous Growth of Highly Conductive Two-Dimensional $TiSi_2$ Nanonets. *Angew. Chem., Int. Ed.* **2008**, *47*, 7681−7684.

(19) Zhou, S.; Liu, X.; Wang, D. Si/$TiSi_2$ Heteronanostructures As High-Capacity Anode Material for Li-Ion Batteries. *Nano Lett.* **2010**, *10*, 860−863.

(20) Merzougui, B., Halalay, I. C., Johnson, J. T., Garabedian, G. C., Balogh, M. P., Swathirajan, S. Supports for fuel cell catalysts based on transition metal silicides. U.S. Patent 0,118,818 A1, 2008, pp 1−4.

(21) Morikawa, Y. Catalysis by Metal Ions Intercalated in Layer Lattice Silicates. *Adv. Catal.* **1993**, *39*, 303−327.

(22) de Gennes, P. G. Soft Matter. *Science* **1992**, *256*, 495−497.

(23) de Gennes, P. G. Soft Matter. *Rev. Mod. Phys.* **1992**, *64*, 645−648.

(24) Xu, C.; Wang, B.; Sun, S. Dumbbell-Like Au-Fe_3O_4 Nanoparticles for Target-Specific Platin Delivery. *J. Am. Chem. Soc.* **2009**, *131*, 4216−4217.

DOI: 10.1021/acsami.7b15682
ACS Appl. Mater. Interfaces 2018, 10, 10771−10777

(25) Zhong, Y.; Abou-Rachid, H.; Lussier, L.-S. Synthesis of High Nitrogen-Doping of Carbon Nanotubes and Modeling the Stabilization of Filled DAATO@CNTs (10, 10) for Nanoenergetic Materials. *J. Phys. Chem. Solids* **2010**, *71*, 134−139.
(26) Yang, D.; Sun, S.; Meng, H.; Dodelet, J.-P.; Sacher, E. Formation of Porous Platinum Nanoparticle Froth for Electrochemical Applications, Produced Without Templates, Surfactants, or Stabilizers. *Chem. Mater.* **2008**, *20*, 4677−4681.
(27) Zhang, J.; Sasaki, K.; Sutter, E.; Adzic, R. R. Stabilization of Platinum Oxygen-Reduction Electrocatalysts Using Gold Clusters. *Science* **2007**, *315*, 220−222.
(28) Chen, Y.; Wang, J.; Liu, H.; Li, R.; Sun, X.; Ye, S.; Knights, S. Enhanced Stability of Pt Electrocatalysts by Nitrogen Doping in CNTs for PEMFCs. *Electrochem. Commun.* **2009**, *11*, 2071−2076.
(29) Dai, Y.; Lim, B.; Yang, Y.; Cobley, C. M.; Li, W.; Cho, E. C.; Grayson, B.; Fanson, P. T.; Campbell, C. T.; Sun, Y.; Xia, Y. A Sinter-Resistant Catalytic System Based on Pt Nanoparticles Supported on TiO_2 Nanofibers and Covered by Porous Silica. *Angew. Chem., Int. Ed.* **2010**, *49*, 8165−8168.
(30) Che, G.; Lakshmi, B. B.; Fisher, E. R.; Martin, C. R. Carbon Nanotube Membranes for Electrochemical Energy Storage and Production. *Nature* **1998**, *393*, 346−349.
(31) Mancharan, R.; Goodenough, J. B. Methanol Oxidation in Acid on Ordered NiTi. *J. Mater. Chem.* **1992**, *2*, 875−887.
(32) Colmati, F.; Antolini, E.; Gonzalez, E. R. Effect of Temperature on the Mechanism of Ethanol Oxidation on Carbon Supported Pt, PtRu and Pt_3Sn Electrocatalysts. *J. Power Sources* **2006**, *157*, 98−103.
(33) Bommersbach, P.; Mohamedi, M.; Guay, D. Electro-Oxidation of Ethanol at Sputter-Deposited Pt−Sn Catalysts. *J. Electrochem. Soc.* **2007**, *154*, B876−B882.
(34) Elezovic, N. R.; Radmilovic, V. R.; Krstajic, N. V. Platinum Nanocatalysts on Metal Oxide Based Supports for Low Temperature Fuel Cell Applications. *RSC Adv.* **2016**, *6*, 6788−6801.
(35) Almeida, T. S.; Garbim, C.; Silva, R. G.; De Andrade, A. R. Addition of Iron Oxide to Pt-Based Catalyst to Enhance the Catalytic Activity of Ethanol Electrooxidation. *J. Electroanal. Chem.* **2017**, *796*, 49−56.

DOI: 10.1021/acsami.7b15682
ACS Appl. Mater. Interfaces 2018, 10, 10771−10777